The behavior of methane/hydrogen/air premixed flame in a closed channel with inhibition

Chao Zhang[a], Xiaobo Shen[a,b*], Jennifer X. Wen[c], Guangli Xiu[a,b,d]

[a] *State Environmental Protection Key Lab of Environmental Risk Assessment and Control on Chemical Processes, School of Resources & Environmental Engineering, East China University of Science and Technology, Shanghai 200237, PR China.*

[b] *Shanghai Institute of Pollution Control and Ecological Security, Shanghai, 200092, PR China*

[c] *Warwick FIRE, School of Engineering, University of Warwick, Coventry, CV4 7AL, UK*

[d] *Shanghai Environmental Protection Key Laboratory on Environmental Standard and Risk Management of Chemical*

Corresponding author: Xiaobo Shen (ustcshenxb@gmail.com); Tel: +86-18521032895

Abstract

Hydrogen enriched natural gas (HNG) is a promising alternative fuel. But the blended fuel will inevitably have different ignition and combustion characteristics as compared to natural gas. The extent of the resulting difference depends on the percentage of hydrogen addition. It may affect the compatibility of combustion systems and have safety implications. The present study was aimed at enhancing the safety of HNG through inhibition by inert gases. Laboratory tests were conducted for methane/hydrogen/air premixed flame propagating in a closed channel with either nitrogen (N_2) or carbon dioxide (CO_2) as the inhibitor. Mixtures with different hydrogen volumetric fractions in fuel, including 0%, 20%, 50% or 80% were investigated. The flame shape evolution and the overpressure in the channel were recorded by high-speed Schlieren

photography and pressure sensor, respectively. The flame shape was found to change in various ways depending on the inhibitor and hydrogen content. The pressure wave had remarkable impacts on flame and pressure dynamics. The effect of buoyancy on the flame deformation was observed and discussed. Both N_2 and CO_2 were found to have considerable inhibition effect on the flame speed and overpressure build-up in the channel while the inhibiting effect of CO_2 was stronger. The inhibition mechanisms of either N_2 or CO_2 were revealed from thermal and kinetic aspects.

Keywords: HNG, Premixed flame, Inhibition, Buoyancy, Mechanism

1 Introduction

Hydrogen enriched natural gas (HNG) is a promising alternative fuel. It was proved that the hydrogen addition (enrichment) can overcome the shortages of NG combustion system, such as high ignition energy, local flame extinction, low power output [1, 2] and significantly enhance the flame dynamics and combustion efficiency [3, 4]. Besides, due to its composition of only natural gas and hydrogen, the combustion of HNG mainly yields CO_2 and H_2O with constraint pollutant released. Given the series of environmental problems associated with fossil fuel, the HNG certainly has an excellent prospect as energy carrier in the near future. However, the mixed fuel will inevitably have different ignition and combustion characteristics as compared to natural gas. The extent of the resulting difference will depend on the percentage of hydrogen addition. It may affect the compatibility of the combustion systems and have safety implications.

From the safety perspective, both hydrogen and natural gas are highly flammable. Hydrogen is featured with low ignition energy, broad flammable range and large burning velocity [5, 6].

Therefore, the potential fire and explosion hazards related to HNG need to be evaluated. Particularly in confined spaces, once the HNG is exposed to air, a combustive mixture will be formed, which can be easily ignited, resulting in fire or explosion. Flame propagation in confined spaces is complicated by flame instability, pressure wave and boundary effect, etc. [7-9]. Confinement can generally promote flame acceleration and even induce deflagration to detonation transition (DDT) as a consequence [10]. At laboratory scale, flame propagation is usually investigated in channels simulating the confined spaces. For example, Mallard and Le Chatelier [11] reported their pioneering work in 1883, which captured a special flame structure in a long channel, namely, the flame front was irregular and would invert itself on the centreline. Thereafter, Ellis [12] took the first photograph of the inverted flame in the channel in 1928. Salamandra et al. [13] named this featured flame shape as “tulip flame”. Until 1990s, Clanet and Searby [14] distinguished four characteristic stages of flame deformation in channels, including spherical flame expansion, finger-shaped flame acceleration, flame-side wall contact and the tulip inversion. In recent years, the flame acceleration with shape changes attracted continuous attention in the area of combustion and explosions. For instance, Zhang et al. [15] found the varied structures of flame front during propagation in vented channel during their experimental and numerical investigations. Yu et al. [16-19] conducted a series of experiments in both closed and half-open channels to investigate the flame behaviour for methane, hydrogen and syngas in air. Xiao et al. [20] numerically investigated the influence of pressure wave on the stability of flame propagation in channels and found out that the Rayleigh-Taylor instability mainly causes the initiation of distorted tulip flame. Obviously from previous studies, the flame propagation in

confined spaces was very complex accompanied by drastic flame deformation and acceleration, which could result in violent pressure rise as well.

For safety consideration, it is beneficial to develop measures that can inhibit potential flame acceleration during combustion. The addition of some inhibitor is useful to constrain the flame and pressure dynamics in combustion. Many studies on the inhibiting effect of inert gas, water mist, powder and halogenated compounds have been carried out. For instance, Benedetto et al. [21] conducted explosion tests of $CH_4/O_2/N_2/CO_2$ and $H_2/O_2/N_2/CO_2$ in a closed cylindrical chamber. The results illustrated that the addition of CO_2 influenced the ignition, laminar burning velocity, flame temperature and combustion rate. Shen et al. [22] discussed the inhibiting effect and mechanism of N_2 or CO_2 on C_2H_4/N_2O mixture explosion at various initial pressures. Explosion mitigation by water mist was examined for methane/air explosion in the tube by Wang et al. [23] in varied droplet sizes and pipe sizes. Yang et al. [24] built an inhibition model for water mist. Pei et al. [25] discussed the synergistic inhibition of inert gas and ultrafine water mist and proposed a promoted inhibiting effect of gas-liquid two phase medium. Yu et al. [26] compared the performance of Urea, $Al(OH)_3$ and $Mg(OH)_2$ on gas explosion. Dounia et al. [27] investigated the sodium bicarbonate powder on flame propagation inhibition by theoretical analysis and simulation. The combined effect of water/sodium chloride mist on the methane/air explosion was explored by Cao et al. [28]. Linteris and Truett [29] considered the inhibiting effect of fluoromethanes (CH_2F_2, CF_3H or CF_4) on the burning velocity by calculations and measurements. The numerical study of the inhibiting efficiency of halogenated compounds (CF_3Br, CF_3I, CF_3H, C_2HF_5, C_2F_6 or CF_4) was elucidated by Noto et al. [30]. These studies identified potential inhibitors and initiated the discussion about the underlying mechanism. Among above-mentioned

inhibitors, N_2 and CO_2 have the advantages of cleanliness, abundant in reserve and low cost [25]. Some previous studies on the inhibiting effect of N_2 or CO_2 for methane/air [31-35], hydrogen/air [36-39] combustion have been conducted. However, as mentioned before, the mixed fuel would have distinct combustion characteristics, and thus would probably give different response to either N_2 or CO_2 inhibition. Therefore, present study aimed to investigate their inhibiting effect on methane/hydrogen/air premixed flame, which is quite beneficial for quantitative assessment on safety measures for HNG utilization.

2 Experimental setup

The experimental setup is shown in Fig. 1, which mainly contains a rectangular channel with an inner cross-section of 25 mm × 25 mm and 300 mm long, a Schlieren system, a high-speed camera (FASTCAM SA2), a pressure sensor, a high-voltage igniter, an oscilloscope, a gas mixing system and a synchronization controller. The bottom and top walls of the channel were made of TP304 stainless steel, while the side walls were entirely replaced by two thick quartzs for optical path of Schlieren photography to capture the whole process of flame evolution from ignition.

The premixed gas mixture was firstly prepared in a gas mixing device then injected into the channel. The mixture was settled for at least 10 min. A pair of spark electrodes were located near the left end wall and the spark gap was rightly on the axis of the channel. The pressure sensor was placed on the top wall near the right end wall.

The testing gas in this study was methane/hydrogen/air mixture with various inhibitor contents (φ_{CO_2} or φ_{N_2}) and hydrogen fractions in fuel (φ_{H_2}), which were defined as follows:

$$\varphi_{N_2} = \frac{V_{N_2}}{V_{mixture}} \quad (1)$$

$$\varphi_{CO_2} = \frac{V_{CO_2}}{V_{mixture}} \quad (2)$$

$$\varphi_{H_2} = \frac{V_{H_2}}{V_{H_2}+V_{CH_4}} \quad (3)$$

where V_{N_2}, V_{CO_2}, V_{H_2}, V_{CH_4} and $V_{mixture}$ were the volumes of nitrogen, carbon dioxide, hydrogen, methane and the testing gas mixture, respectively. The purity of gases used in this work were 99.98% for CO_2, 99.98% for N_2, 99.90% for air, 99.99% for H_2 and 99.99% for CH_4. The experiments were repeated at least three times to ensure the repeatability and the measurement uncertainty of the pressure sensor was ±1%. The initial conditions were 298 K and 101325 Pa.

3 Flame shape evolution

Experiments were conducted for premixed methane/air flame inhibited by 0%-20% N_2 and 0%-20% CO_2. Examples of the entire process of flame evolution recorded by the high-speed Schlieren photography are shown in Fig. 2, which captured the four-stage flame deformation defined by Clanet and Searby [14]. The flame expanded spherically right after ignition. After a short period, due to the confinement of the wall, the flame was gradually stretched into a finger shape. Then the skirt of the flame touched the sidewall. The flame-wall contact points moved along the wall fast catching the flame tip on the centreline. Eventually, the flame front turned into a plane shape and immediately after this, the flame front inverted forming a cusp towards the burnt gas. A classic tulip flame came into being. With the increase of inhibitor content, the moment when these characteristic structures were formed delayed.

Following the classic tulip inversion, some peculiar flame shapes appeared under certain conditions as shown in Figs. 3a and 3b. With the same inhibiting condition, the extent of flame deformation was stronger for mixtures with higher hydrogen content. For instance, the pure methane flame maintained its tulip shape until quenching in the absence of inhibition. When the hydrogen content, φ_{H_2} was increased to 20%, a few wrinkles appeared on the tulip flame lips. When φ_{H_2} was increased to 50%, some new cusps emerged near the sidewalls and they moved along the flame front towards the primary cusp. Such phenomenon was referred to as "cloudy flame" in our previous publication [40]. With φ_{H_2} reached 80% in the absence of inhibition, the flame shape underwent a more complicated deformation including elongated tulip shape, T-shape [5], and cellular flame [41] until the end. With the inhibition of N_2 or CO_2, the flame structures were more stable. For example, for φ_{H_2} = 50% and 10% N_2 addition, the flame maintained the classic tulip flame until the end without changing to "cloudy flame". In almost all cases, the flame propagated faster near the upper wall (e.g. at 61.90 ms with 10% N_2 and φ_{H_2} = 0% in Fig. 3a). This was thought to be due to the buoyancy effects: firstly, as the density of N_2 (or CO_2) is higher than that of CH_4 and H_2 mixtures, concentration gradients would be built up with time leading to relatively higher H_2 content near the top and higher N_2 fraction near the bottom. Thus, the inhibition was stronger on the flame near the bottom. Such effect was, however, less obvious for the cases with 80% H_2 within the range of N_2 fractions investigated, this was thought to be due to the higher flame speeds and relatively shorter physical times within the channel during which the concentration gradients were not sufficiently developed. Secondly, the flame with inhibition was slowed down, during which the movement of burnt gas affected by buoyancy

became more and more apparent. Therefore, the flame propagated obliquely with resultant force from buoyancy and combustion.

4. Flame dynamics

4.1 Flame propagation speed

Figure 4 shows the propagation speed of flame forefront versus time with varied hydrogen or inhibitor concentrations. All the flames accelerated at the early stage until reaching the maximum. With either increase of inhibitor content or decrease of φ_{H_2}, the occurrence of maximum flame propagation speed (v_{max}) delayed accordingly. After that, the propagation speed fluctuated with time accompanying the flame shape changes. At the condition of φ_{H_2} = 80% and 0% inhibitor, the propagation speed of the flame forefront fluctuated most drastically and even receded with negative propagation speed. As discussed in our previous study [40], at conditions with high hydrogen content, relatively stronger pressure waves which also propagated faster were reflected from the end of the channel, pushing back the unburnt gas with the effect of causing the flame to propagate backwards. Besides, the loss of the flame area caused by the flame-wall contacting was also an important factor affecting the flame propagation speed. It is noteworthy that the maximum flame propagation speed always appeared at the moment after the flame first touching the sidewall. This indicated that the flame speed did not decrease immediately upon touching the wall. But due to the loss of flame surface area, the acceleration was believed to decline immediately. The flame speed decrease caused by N_2 or CO_2 addition underwent different tendency. Take the condition of φ_{H_2} = 20% as example. The decrement of v_{max} with addition of N_2 or CO_2 is shown in Table 1. With the same addition of N_2 or CO_2, the v_{max}

was always lower with CO_2 dilution. However, the decrement of flame speed at the condition of 10%-20% CO_2 was lower than that at the condition of 10%-20% N_2, though the value of v_{max} with CO_2 dilution was still smaller. This phenomenon was different from the linear relationship between flame speed and inhibitor content in several previous studies [42-46] on laminar flame, which may be attributed to the effect of wall interaction in this channel. However, the laminar flame speed calculated and discussed in the later section presented similar descending trend with those in previous studies [42-46].

Table 1. The decrement of v_{max} with addition of N_2 or CO_2.

Inhibitor content, %	Inhibited by N_2, φ_{H_2} = 20%		Inhibited by CO_2, φ_{H_2} = 20%	
	$v_{max,}$ m/s	Decrement, m/s	v_{max}, m/s	Decrement, m/s
0	22.76	/	22.76	/
5	16.58	6.18	12.11	10.65
10	13.05	3.53	4.24	7.87
15	8.08	4.97	3.08	1.16
20	5.75	2.33	1.32	1.76

4.2 Overpressure dynamics

The overpressure in the channel is shown in Fig. 5. It rose rapidly following ignition before reaching its maximal value. With the increase of inhibitor content, the maximum overpressure decreased, and its arrival time was delayed. Analogous to the flame propagation speed, the overpressure rose and fluctuated more gently with increasing inhibitor content or decreasing

hydrogen fraction. As illustrated in Fig. 6, with CO_2 addition, the maximum overpressure was lower than that with N_2 addition for the same fuel composition.

5 Inhibiting mechanism of N_2 and CO_2

5.1 Thermal diffusivity

Thermal diffusivity is an important parameter to describe the heat transport in materials [47]. The decrease of thermal diffusivity would lead to the inhibition of flame propagation [48]. Figure 7 shows the thermal diffusivity versus inhibitor content with different hydrogen addition. It can be seen that the thermal diffusivity decreased with the increase of N_2 or CO_2, indicating that the addition of N_2 or CO_2 leads to reduction in the thermal diffusivity, resulting in the inhibition of flame propagation. The addition of CO_2 had stronger effect in reducing the thermal diffusivity and hence stronger inhibition effect. With the increase of φ_{H_2} and constant inhibitor content, the thermal diffusivity increased.

5.2 Thermal conductivity

On the other hand, the thermal conductivity is another property affecting the laminar flame speed of the premixed flame [49]. The computed thermal conductivity values for the mixtures considered are plotted in Fig. 8. As expected, with the increase of φ_{H_2} and constant inhibitor content, the thermal conductivity and laminar flame speed both increased. With the increase of inhibitor content, the thermal conductivity decreased resulting in lower laminar flame speed shown in Fig. 9. CO_2 had more profound effect on reducing the thermal conductivity and hence stronger inhibition effect.

5.3 Laminar flame speed

The laminar flame speed versus time is shown in Fig. 9. The laminar flame speed decreased almost linearly with N_2 addition. However, with CO_2 addition, it decreased monotonically in a curve shape with the decrement reduced with gradual increasing CO_2 content. But CO_2 dilution always led to lower laminar flame speed than N_2 dilution at the same content.

5.4 Flame thickness

Flame thickness has inhibiting effect on the hydrodynamic instability which influences the flame front stability [50, 51], i.e. the increase of flame thickness can lead to more stable flame evolution, i.e. presenting less flame shape changes. Flame thickness was calculated as follows [48, 52]:

$$\alpha = \frac{\lambda}{\rho_u \cdot C_p} \tag{4}$$

$$\delta = \frac{2\lambda}{\rho_u \cdot C_p \cdot S_L} \left(\frac{T_{ad}}{T_0}\right)^{0.7} \tag{5}$$

where the α, λ, ρ_u, C_p, δ, S_L, T_{ad} and T_0 were thermal diffusivity, thermal conductivity, unburnt mixture density, specific heat, flame thickness, laminar flame speed, adiabatic flame temperature and initial temperature of unburnt mixture, respectively. The calculation of laminar flame speed was based on HP-Mech [53] using CHEMKIN Pro software [54]. The other parameters were calculated by GASEQ [55] using chemical equilibrium method. As shown in Fig. 10, the flame thickness was enlarged with increasing inhibitor content, which would stabilize the flame front against instabilities, as can be seen from flame images above. The increase of flame thickness

was more prominent with higher inhibitor content. In general, the flame deformation would be attenuated due to the thickening of flame front by N_2 or CO_2 addition, especially with CO_2.

5.5 Kinetic effect and Adiabatic flame temperature

Firstly, due to the third-body collisional effect, the addition of N_2 or CO_2 would enhance two of the sensitive reactions for ignition ($H + O_2 + M = HO_2 + M$, $CH_3 + CH_3 + M = C_2H_6 + M$) and one of the sensitive reactions for laminar flame speed ($H + O_2 + M = HO_2 + M$) [56]. M is the third body and characterized by collisional efficiency. The reaction of $CH_3 + CH_3 + M$ is a chain-terminating step, which would inhibit the combustion by producing relatively stable compound of C_2H_6 in the radical pool. The reaction ($H + O_2 + M = HO_2 + M$) will compete for highly active H radical with the reaction ($H + O_2 = O + OH$) and produce less active HO_2 radical [57]. As a result, the inhibitor addition would result in weakened combustion and flame propagation. In both reaction paths, the collisional efficiency of CO_2 is greater than that of N_2 [53]. Besides, it is noteworthy that CO_2 also acted as a main reactant in the path of ($CO + OH = H + CO_2$) which is a very important reaction in combustion chemistry [45, 58]. Evidently, the addition of CO_2 would reverse the reaction ($CO + OH = H + CO_2$), which competed for extra H radical with ($H + O_2 = O + OH$) resulting in reductions of important radicals of O, H, and OH [58]. Therefore, compared to N_2, CO_2 had more pronounced inhibiting kinetics. Further, it could also infer that with higher hydrogen content, the advantage of CO_2 inhibition would be more enhanced since the pathways evolving H radical are of such great importance. The experimental results give some proofs in Fig. 6 that the inhibition discrepancy between N_2 and CO_2 on maximum overpressure was enlarged with 80% H_2 content.

The reduced adiabatic flame temperature can manifest the inhibited kinetics, which was calculated using the chemical equilibrium method [55] as shown in Fig. 11. The mixture with CO_2 addition at the same amount had lower flame temperature as expected. Nevertheless, it needs to mention that, besides the kinetic effect, both CO_2 and N_2 can reduce flame temperature with their high specific heat. Comparatively, CO_2 has larger specific heat than N_2 [42, 49]. As suggested by Law [49] and Hu et al. [44], the adiabatic flame temperature is closely related to laminar flame speed. Therefore, according to Eq. (5), the decreasing of adiabatic flame temperature would remarkably thicken the flame front.

6 Conclusions

The flame propagation of methane/hydrogen/air mixture was studied in a closed channel with inhibitor (N_2 or CO_2) addition. The hydrogen fractions in the fuel mixture were 0%, 20%, 50% and 80% by volume. For different φ_{H_2} and inhibitor contents, different flame evolution processes were observed.

Either increasing the inhibitor content or decreasing φ_{H_2} could remarkably decrease the flame propagation speed and the overpressure. At the same φ_{H_2} and inhibitor content, CO_2 had more profound inhibition effect on flame acceleration and overpressure rise.

Thermal analysis showed that the addition of N_2 and CO_2 would decrease thermal diffusivity and thermal conductivity, resulting in the reduction of laminar flame speed. The addition of the inhibitor resulted in the increase of flame thickness, which attenuated the flame deformation and consequently supressed the flame acceleration. The inhibitor could also decrease the adiabatic flame temperature by inhibited kinetics and high specific heat. Compared to N_2, the

mixture with CO_2 addition has lower thermal diffusivity, conductivity and laminar flame speed, smaller adiabatic flame temperature and larger flame thickness.

Kinetic analysis showed that both N_2 and CO_2 addition could inhibit the chemical process due to their collisional effect on key elementary reactions including $H + O_2 + M = HO_2 + M$, $CH_3 + CH_3 + M = C_2H_6 + M$. The collisional efficiency of CO_2 is higher than N_2. Additionally, CO_2 could reverse the reaction ($CO + OH = H + CO_2$) effectively consuming extra H atom. Therefore, CO_2 has more pronounced inhibition kinetics than that of N_2.

Acknowledgments

The authors gratefully acknowledge the financial support of National Natural Science Foundation of China (Grant No. 51604121).

References

[1] Wang J, Huang Z, Tang C, Miao H, Wang X. Numerical study of the effect of hydrogen addition on methane–air mixtures combustion. International Journal of Hydrogen Energy 2009;34(2):1084-96.
[2] Shen X, Xiu G, Wu S. Experimental study on the explosion characteristics of methane/air mixtures with hydrogen addition. Applied Thermal Engineering 2017;120:741-7.
[3] Wang J, Huang Z, Tang C, Zheng J. Effect of hydrogen addition on early flame growth of lean burn natural gas–air mixtures. International Journal of Hydrogen Energy 2010;35(13):7246-52.
[4] Yu H, Hu E, Cheng Y, Yang K, Zhang X, Huang Z. Effects of hydrogen addition on the laminar flame speed and markstein length of premixed dimethyl ether-air flames. Energy and Fuels 2015;29(7):4567-75.
[5] Shen X, Zhang C, Xiu G, Zhu H. Evolution of premixed stoichiometric hydrogen/air flame in a closed duct. Energy 2019;176:265-71.
[6] Xiao H, Duan Q, Sun J. Premixed flame propagation in hydrogen explosions. Renewable and Sustainable Energy Reviews 2018;81:1988-2001.
[7] Nishimura I, Mogi T, Dobashi R. Simple method for predicting pressure behavior during gas explosions in confined spaces considering flame instabilities. Journal of Loss Prevention in the Process Industries 2013;26(2):351-4.
[8] Yang X, Yu M, Zheng K, Wan S, Wang L. A comparative investigation of premixed flame propagation behavior of syngas-air mixtures in closed and half-open ducts. Energy 2019;178:436-46.

[9] Fernández-Galisteo D, Kurdyumov VN, Ronney PD. Analysis of premixed flame propagation between two closely-spaced parallel plates. Combustion and Flame 2018;190:133-45.
[10] Rudy W, Zbikowski M, Teodorczyk A. Detonations in hydrogen-methane-air mixtures in semi confined flat channels. Energy 2016;116:1479-83.
[11] Mallard E, Le Chatelier H. Combustion of explosive gas mixtures. Ann mines 1883;8:274.
[12] Ellis OdC. Flame movement in gaseous explosive mixtures. J Fuel Sci 1928;7:502-8.
[13] Salamandra G, Bazhenova T, Naboko I. Seventh Symposium (International) on Combustion. Butterworth and Company, Ltd, London 1959;5:321.
[14] Clanet C, Searby G. On the "tulip flame" phenomenon. Combustion and flame 1996;105(1-2):225-38.
[15] Zhang Y, Jiao F, Huang Q, Cao W, Shi L, Zhao M, et al. Experimental and numerical studies on the closed and vented explosion behaviors of premixed methane-hydrogen/air mixtures. Applied Thermal Engineering 2019;159.
[16] Yu M, Yang X, Zheng K, Zheng L, Wen X. Experimental study of premixed syngas/air flame deflagration in a closed duct. International Journal of Hydrogen Energy 2018;43(29):13676-86.
[17] Zheng K, Yu M, Zheng L, Wen X, Chu T, Wang L. Experimental study on premixed flame propagation of hydrogen/methane/air deflagration in closed ducts. International Journal of Hydrogen Energy 2017;42(8):5426-38.
[18] Yu M, Zheng K, Zheng L, Chu T, Guo P. Effects of hydrogen addition on propagation characteristics of premixed methane/air flames. Journal of Loss Prevention in the Process Industries 2015;34:1-9.
[19] Yu M, Zheng K, Zheng L, Chu T, Guo P. Scale effects on premixed flame propagation of hydrogen/methane deflagration. International Journal of Hydrogen Energy 2015;40(38):13121-33.
[20] Xiao H, Houim RW, Oran ES. Effects of pressure waves on the stability of flames propagating in tubes. Proceedings of the Combustion Institute 2017;36(1):1577-83.
[21] Di Benedetto A, Di Sarli V, Salzano E, Cammarota F, Russo G. Explosion behavior of CH4/O2/N2/CO2 and H2/O2/N2/CO2 mixtures. International Journal of Hydrogen Energy 2009;34(16):6970-8.
[22] Shen X, Zhang N, Shi X, Cheng X. Experimental studies on pressure dynamics of C2H4/N2O mixtures explosion with dilution. Applied Thermal Engineering 2019;147:74-80.
[23] Wang F, Yu M, Wen X, Deng H, Pei B. Suppression of methane/air explosion in pipeline by water mist. Journal of Loss Prevention in the Process Industries 2017;49:791-6.
[24] Yang W, Kee RJ. The effect of monodispersed water mists on the structure, burning velocity, and extinction behavior of freely propagating, stoichiometric, premixed, methane-air flames. Combustion and Flame 2002;130(4):322-35.
[25] Pei B, Yu M, Chen L, Wang F, Yang Y, Zhu X. Experimental study on the synergistic inhibition effect of gas-liquid two phase medium on gas explosion. Journal of Loss Prevention in the Process Industries 2017;49:797-804.
[26] Yu M, Wang T, You H, An A. Study on the Effect of Thermal Property of Powder on the Gas Explosion Suppression. Procedia Engineering 2011;26:1035-42.

[27] Dounia O, Vermorel O, Poinsot T. Theoretical analysis and simulation of methane/air flame inhibition by sodium bicarbonate particles. Combustion and Flame 2018;193:313-26.
[28] Cao X, Ren J, Zhou Y, Wang Q, Gao X, Bi M. Suppression of methane/air explosion by ultrafine water mist containing sodium chloride additive. J Hazard Mater 2015;285:311-8.
[29] Linteris GT, Truett L. Inhibition of premixed methane-air flames by fluoromethanes. Combustion and Flame 1996;105(1):15-27.
[30] Noto T, Babushok V, Hamins A, Tsang W. Inhibition effectiveness of halogenated compounds. Combustion and Flame 1998;112(1):147-60.
[31] Kim SG, Lee DK, Noh D-S. An experimental study ofN2dilution effects onCH4–O2flame stabilization characteristics in a two-section porous medium. Applied Thermal Engineering 2016;103:1390-7.
[32] Yang J, Gong Y, Guo Q, Zhu H, He L, Yu G. Dilution effects of N2 and CO2 on flame structure and reaction characteristics in CH4/O2 flames. Experimental Thermal and Fluid Science 2019;108:16-24.
[33] Chan YL, Zhu MM, Zhang ZZ, Liu PF, Zhang DK. The Effect of CO2 Dilution on the Laminar Burning Velocity of Premixed Methane/Air Flames. Energy Procedia 2015;75:3048-53.
[34] Wang Z, Zuo H, Liu Z, Li W, Dou H. Impact of N2 dilution on combustion and emissions in a spark ignition CNG engine. Energy Conversion and Management 2014;85:354-60.
[35] Khan AR, Anbusaravanan S, Kalathi L, Velamati R, Prathap C. Investigation of dilution effect with N2/CO2 on laminar burning velocity of premixed methane/oxygen mixtures using freely expanding spherical flames. Fuel 2017;196:225-32.
[36] Grosseuvres R, Comandini A, Bentaib A, Chaumeix N. Combustion properties of H2/N2/O2/steam mixtures. Proceedings of the Combustion Institute 2019;37(2):1537-46.
[37] Paidi SK, Bhavaraju A, Akram M, Kumar S. Effect of N2/CO2 dilution on laminar burning velocity of H2–air mixtures at high temperatures. International Journal of Hydrogen Energy 2013;38(31):13812-21.
[38] Holborn PG, Battersby P, Ingram JM, Averill AF, Nolan PF. Modelling the mitigation of hydrogen deflagrations in a vented cylindrical rig with water fog and nitrogen dilution. International Journal of Hydrogen Energy 2013;38(8):3471-87.
[39] Shi B, Li B, Zhao X, Chen R, Fujita O, Wang N. Rapidly mixed combustion of hydrogen/oxygen diluted by N2 and CO2 in a tubular flame combustor. International Journal of Hydrogen Energy 2018;43(31):14806-15.
[40] Zhang C, Wen J, Shen X, Xiu G. Experimental study of hydrogen/air premixed flame propagation in a closed channel with inhibitions for safety consideration. International Journal of Hydrogen Energy 2019.
[41] Gonzalez M. Acoustic instability of a premixed flame propagating in a tube. Combustion and Flame 1996;107:245-59.
[42] Chen Z, Wei L, Huang z, Miao H, Wang X, Jiang D. Measurement of laminar burning velocities of dimethyl ether-air premixed mixtures with N_2 and CO_2 dilution. Enerry & Fuel 2009;23:735-9.
[43] Li Q, Fu J, Wu X, Tang C, Huang Z. Laminar Flame Speeds of DMF/Iso-octane-Air-N2/CO2 Mixtures. Energy & Fuels 2012;26(2):917-25.

[44] Hu E, Jiang X, Huang Z, Iida N. Numerical Study on the Effects of Diluents on the Laminar Burning Velocity of Methane–Air Mixtures. Energy & Fuels 2012;26(7):4242-52.
[45] Chen Z, Tang C, Fu J, Jiang X, Li Q, Wei L, et al. Experimental and numerical investigation on diluted DME flames: Thermal and chemical kinetic effects on laminar flame speeds. Fuel 2012;102:567-73.
[46] Cai X, Wang J, Zhao H, Zhang M, Huang Z. Flame morphology and self-acceleration of syngas spherically expanding flames. International Journal of Hydrogen Energy 2018;43(36):17531-41.
[47] Naseem H, Murthy H. A simple thermal diffusivity measurement technique for polymers and particulate composites. International Journal of Heat and Mass Transfer 2019;137:968-78.
[48] Li Y, Bi M, Yan C, Liu Q, Zhou Y, Gao W. Inerting effect of carbon dioxide on confined hydrogen explosion. International Journal of Hydrogen Energy 2019.
[49] Law CK. COMBUSTION PHYSICS. Cambridge University Press; 2006.
[50] Vu TM, Park J, Kim JS, Kwon OB, Yun JH, Keel SI. Experimental study on cellular instabilities in hydrocarbon/hydrogen/carbon monoxide–air premixed flames. International Journal of Hydrogen Energy 2011;36(11):6914-24.
[51] Miao J, Leung CW, Huang Z, Cheung CS, Yu H, Xie Y. Laminar burning velocities, Markstein lengths, and flame thickness of liquefied petroleum gas with hydrogen enrichment. International Journal of Hydrogen Energy 2014;39(24):13020-30.
[52] Poinsot T, Veynante D. Theoretical and Numerical Combustion. philadelphia: (2nd ed.), Edwards RT Inc; 2005.
[53] Shen X, Yang X, Santner J, Sun J, Ju Y. Experimental and kinetic studies of acetylene flames at elevated pressures. Proceedings of the Combustion Institute 2015;35(1):721-8.
[54] ChemKin Pro Reaction design. San Diego; 2013.
[55] Morley C. Gaseq.A Chemical Equilibrium Program for Windows.
[56] Li R, He G, Qin F, Pichler C, Konnov AA. Comparative analysis of detailed and reduced kinetic models for CH4 + H2 combustion. Fuel 2019;246:244-58.
[57] Qiao L, Gu Y, Dahm WJA, Oran ES, Faeth GM. Near-limit laminar burning velocities of microgravity premixed hydrogen flames with chemically-passive fire suppressants. Proceedings of the Combustion Institute 2007;31(2):2701-9.
[58] Zeng W, Ma H, Liang Y, Hu E. Experimental and modeling study on effects of N2 and CO2 on ignition characteristics of methane/air mixture. J Adv Res 2015;6(2):189-201.

Figure captions:

Fig. 1 Experimental apparatus.

Fig. 2 Flame evolution in the channel (a: inhibited by N_2; b: inhibited by CO_2).

Fig. 3 The flame evolution in the channel at later stages with hydrogen addition (a: inhibited by N_2; b: inhibited by CO_2).

Fig. 4 Flame propagation velocity versus time with varied φ_{H_2} or inhibitor addition (a, b: φ_{H_2} = 0%; c, d: φ_{H_2} = 20%; e, f: φ_{H_2} = 50%; g, h: φ_{H_2} = 80%; a, c, e, g: inhibited by N_2; b, d, f, h: inhibited by CO_2).

Fig. 5 Overpressure in the channel versus time with varied φ_{H_2} and inhibitor content (a, b: φ_{H_2} = 0%; c, d: φ_{H_2} = 20%; e, f: φ_{H_2} = 50%; g, h: φ_{H_2} = 80%; a, c, e, g: inhibited by N_2; b, d, f, h: inhibited by CO_2).

Fig. 6 Maximum overpressure versus inhibitor content (a: φ_{H_2} = 0%; b: φ_{H_2} = 20%; c: φ_{H_2} = 50%; d: φ_{H_2} = 80%).

Fig. 7 Thermal diffusivity versus inhibitor content with varying φ_{H_2}.

Fig. 8 Thermal conductivity versus inhibitor content with varying φ_{H_2}.

Fig. 9 Laminar flame speed versus inhibitor content with varying φ_{H_2}

Fig. 10 Flame thickness versus inhibitor content with varying φ_{H_2}.

Fig. 11 Adiabatic temperature versus inhibitor content with varying φ_{H_2}.

Fig. 1

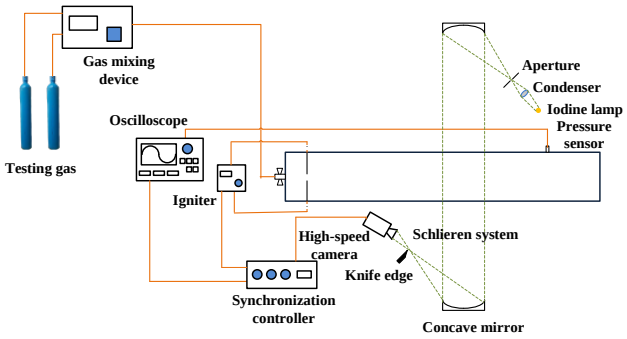
Gas mixing device
Testing gas
Oscilloscope
Igniter
Aperture
Condenser
Iodine lamp
Pressure sensor
High-speed camera
Schlieren system
Knife edge
Synchronization controller
Concave mirror

Fig. 2

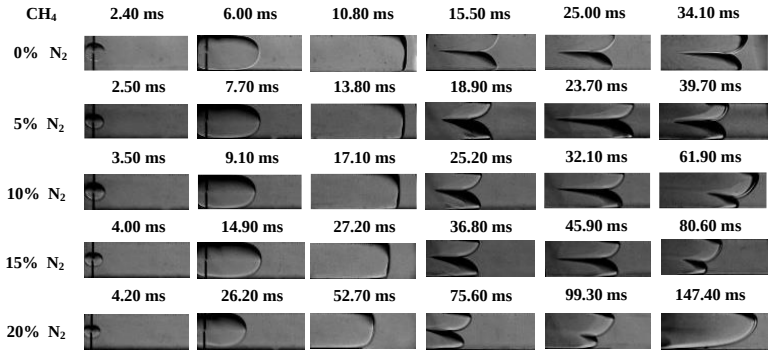
CH4
2.40 ms
6.00 ms
10.80 ms
15.50 ms
25.00 ms
34.10 ms
0% N2
2.50 ms
7.70 ms
13.80 ms
18.90 ms
23.70 ms
39.70 ms
5% N2
3.50 ms
9.10 ms
17.10 ms
25.20 ms
32.10 ms
61.90 ms
10% N2
4.00 ms
14.90 ms
27.20 ms
36.80 ms
45.90 ms
80.60 ms
15% N2
4.20 ms
26.20 ms
52.70 ms
75.60 ms
99.30 ms
147.40 ms
20% N2

(a)

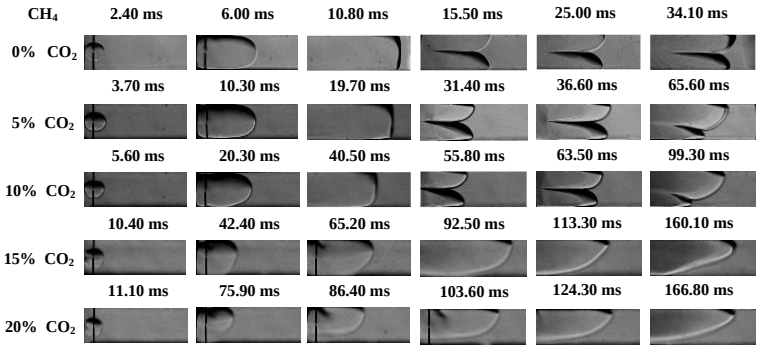
CH4
2.40 ms
6.00 ms
10.80 ms
15.50 ms
25.00 ms
34.10 ms
0% CO2
3.70 ms
10.30 ms
19.70 ms
31.40 ms
36.60 ms
65.60 ms
5% CO2
5.60 ms
20.30 ms
40.50 ms
55.80 ms
63.50 ms
99.30 ms
10% CO2
10.40 ms
42.40 ms
65.20 ms
92.50 ms
113.30 ms
160.10 ms
15% CO2
11.10 ms
75.90 ms
86.40 ms
103.60 ms
124.30 ms
166.80 ms
20% CO2

(b)

Fig. 3

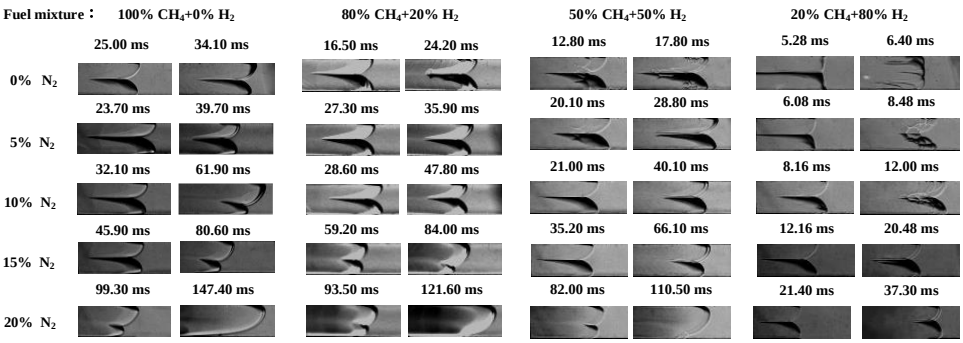
Fuel mixture： 100% CH4+0% H2
80% CH4+20% H2
50% CH4+50% H2
20% CH4+80% H2
0% N2
5% N2
10% N2
15% N2
20% N2
25.00 ms
34.10 ms
16.50 ms
24.20 ms
12.80 ms
17.80 ms
5.28 ms
6.40 ms
23.70 ms
39.70 ms
27.30 ms
35.90 ms
20.10 ms
28.80 ms
6.08 ms
8.48 ms
32.10 ms
61.90 ms
28.60 ms
47.80 ms
21.00 ms
40.10 ms
8.16 ms
12.00 ms
45.90 ms
80.60 ms
59.20 ms
84.00 ms
35.20 ms
66.10 ms
12.16 ms
20.48 ms
99.30 ms
147.40 ms
93.50 ms
121.60 ms
82.00 ms
110.50 ms
21.40 ms
37.30 ms

(a)

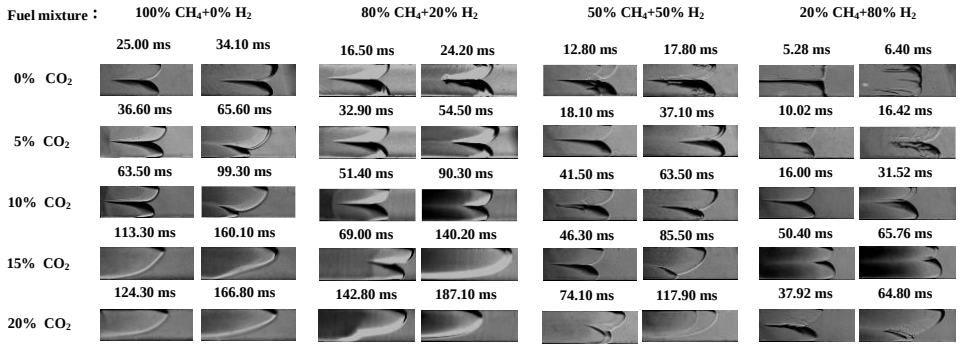
Fuel mixture： 100% CH4+0% H2
80% CH4+20% H2
50% CH4+50% H2
20% CH4+80% H2
0% CO2
5% CO2
10% CO2
15% CO2
20% CO2
25.00 ms
34.10 ms
16.50 ms
24.20 ms
12.80 ms
17.80 ms
5.28 ms
6.40 ms
36.60 ms
65.60 ms
32.90 ms
54.50 ms
18.10 ms
37.10 ms
10.02 ms
16.42 ms
63.50 ms
99.30 ms
51.40 ms
90.30 ms
41.50 ms
63.50 ms
16.00 ms
31.52 ms
113.30 ms
160.10 ms
69.00 ms
140.20 ms
46.30 ms
85.50 ms
50.40 ms
65.76 ms
124.30 ms
166.80 ms
142.80 ms
187.10 ms
74.10 ms
117.90 ms
37.92 ms
64.80 ms

(b)

Fig. 4

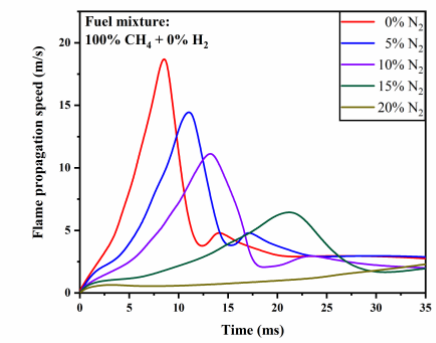
Fuel mixture:
100% CH4 + 0% H2
0% N2
5% N2
10% N2
15% N2
20% N2
Flame propagation speed (m/s)
Time (ms)

(a)

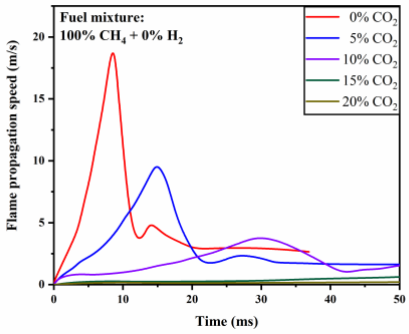
Fuel mixture:
100% CH4 + 0% H2
0% CO2
5% CO2
10% CO2
15% CO2
20% CO2
Flame propagation speed (m/s)
Time (ms)

(b)

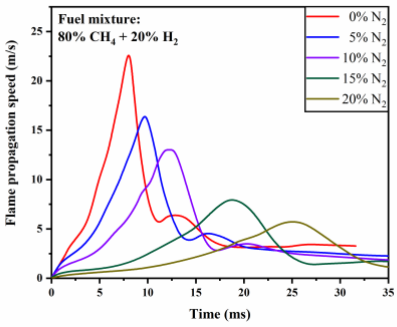
Fuel mixture:
80% CH4 + 20% H2
0% N2
5% N2
10% N2
15% N2
20% N2
Flame propagation speed (m/s)
Time (ms)

(c)

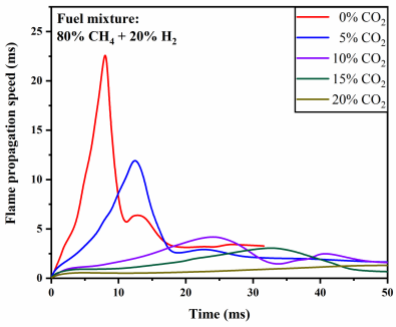
Fuel mixture:
80% CH4 + 20% H2
0% CO2
5% CO2
10% CO2
15% CO2
20% CO2
Flame propagation speed (ms)
Time (ms)

(d)

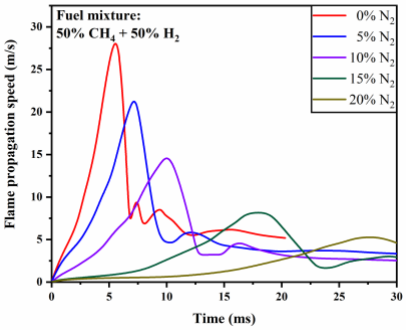
Fuel mixture:
50% CH4 + 50% H2
0% N2
5% N2
10% N2
15% N2
20% N2
Flame propagation speed (m/s)
Time (ms)

(e)

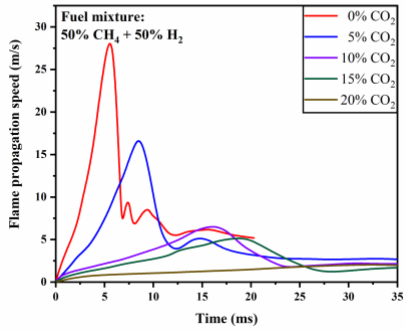
Fuel mixture:
50% CH4 + 50% H2
0% CO2
5% CO2
10% CO2
15% CO2
20% CO2
Flame propagation speed (m/s)
Time (ms)

(f)

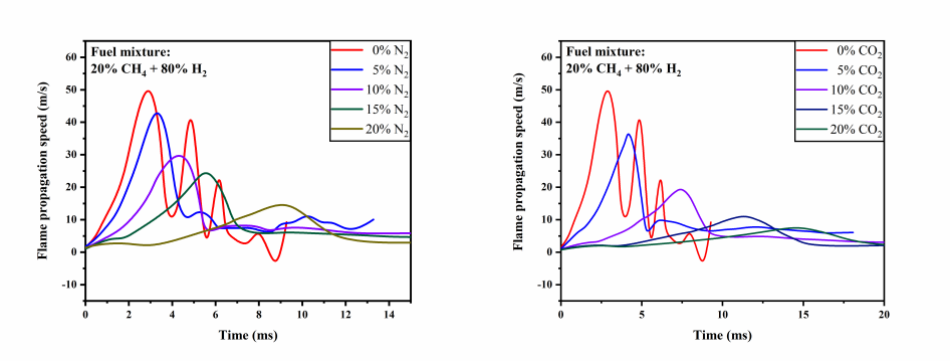
Fuel mixture:
20% CH4 + 80% H2
0% N2
5% N2
10% N2
15% N2
20% N2
Flame propagation speed (m/s)
Time (ms)
Fuel mixture:
20% CH4 + 80% H2
0% CO2
5% CO2
10% CO2
15% CO2
20% CO2
Flame propagation speed (m/s)
Time (ms)

(g) (h)

Fig. 5

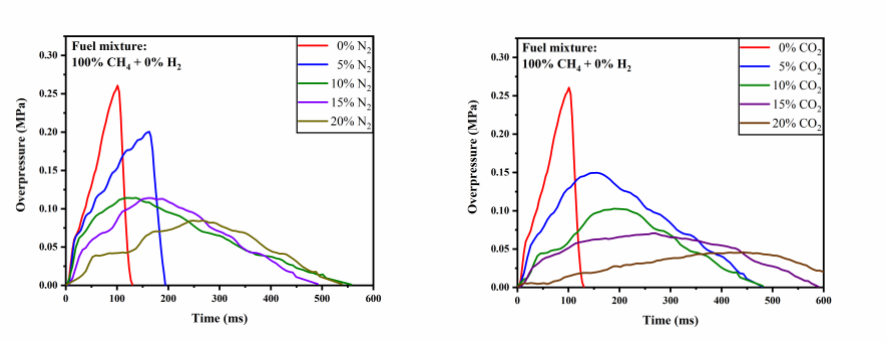
Fuel mixture:
100% CH4 + 0% H2
0% N2
5% N2
10% N2
15% N2
20% N2
Overpressure (MPa)
Time (ms)
Fuel mixture:
100% CH4 + 0% H2
0% CO2
5% CO2
10% CO2
15% CO2
20% CO2
Overpressure (MPa)
Time (ms)

(a) (b)

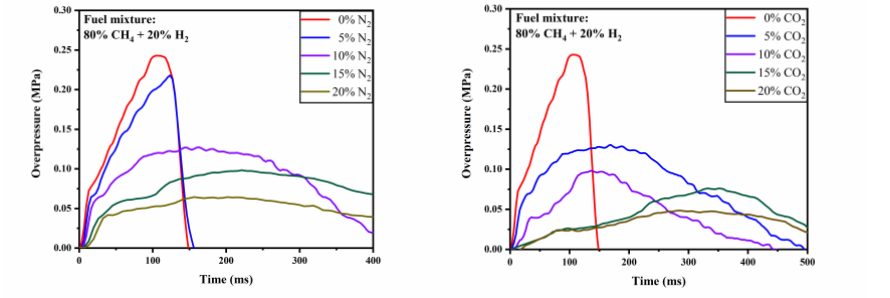
Fuel mixture:
80% CH4 + 20% H2
0% N2
5% N2
10% N2
15% N2
20% N2
Overpressure (MPa)
Time (ms)
Fuel mixture:
80% CH4 + 20% H2
0% CO2
5% CO2
10% CO2
15% CO2
20% CO2
Overpressure (MPa)
Time (ms)

(c) (d)

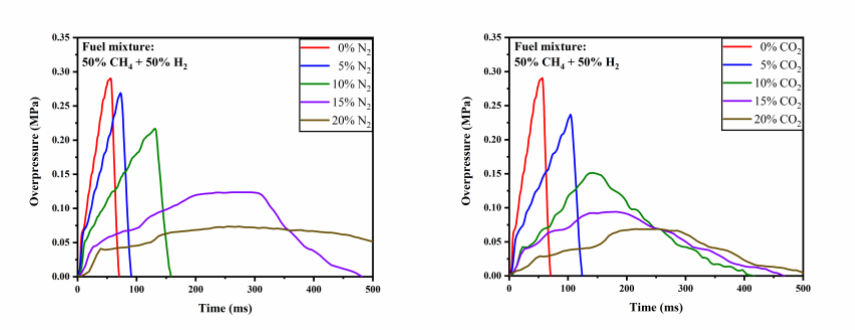
Fuel mixture:
50% CH4 + 50% H2
0% N2
5% N2
10% N2
15% N2
20% N2
Overpressure (MPa)
Time (ms)
Fuel mixture:
50% CH4 + 50% H2
0% CO2
5% CO2
10% CO2
15% CO2
20% CO2
Overpressure (MPa)
Time (ms)

(e) (f)

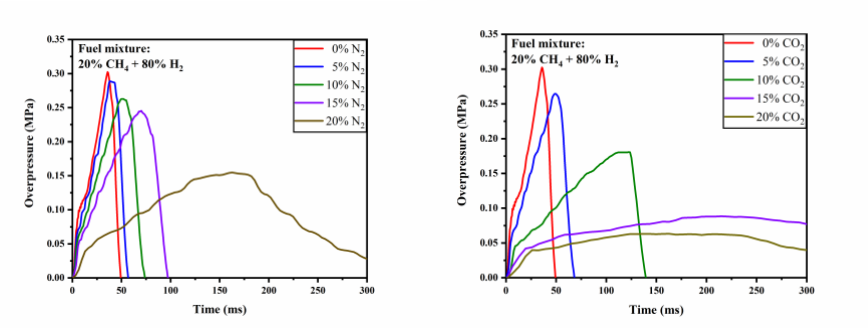
Fuel mixture:
20% CH4 + 80% H2
0% N2
5% N2
10% N2
15% N2
20% N2
Overpressure (MPa)
Time (ms)
Fuel mixture:
20% CH4 + 80% H2
0% CO2
5% CO2
10% CO2
15% CO2
20% CO2
Overpressure (MPa)
Time (ms)

(g) (h)

Fig. 6

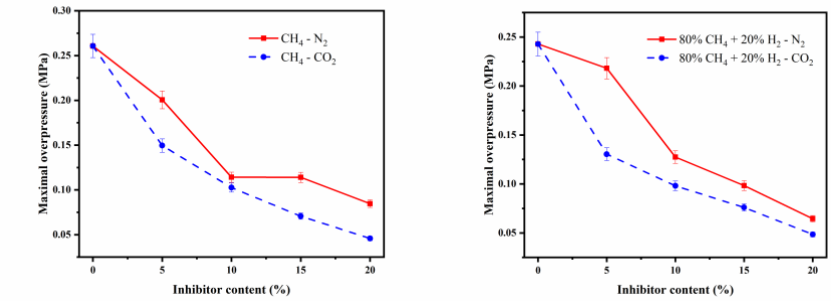
CH4 - N2
CH4 - CO2
Maximal overpressure (MPa)
Inhibitor content (%)
80% CH4 + 20% H2 - N2
80% CH4 + 20% H2 - CO2
Maximal overpressure (MPa)
Inhibitor content (%)

(a) (b)

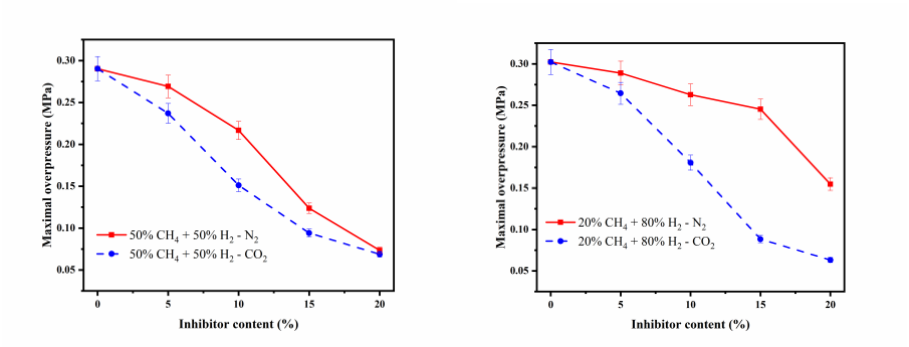
Maximal overpressure (MPa)
Inhibitor content (%)
50% CH4 + 50% H2 - N2
50% CH4 + 50% H2 - CO2
20% CH4 + 80% H2 - N2
20% CH4 + 80% H2 - CO2

(c) (d)

Fig. 7

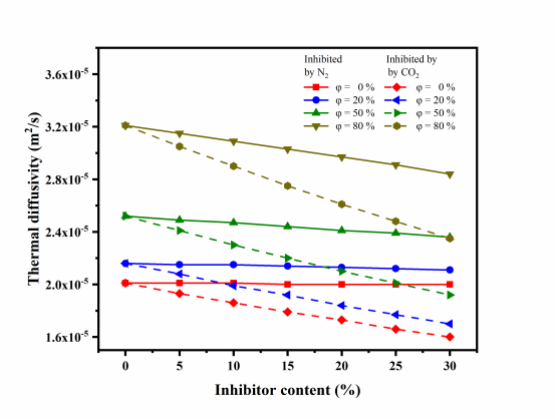
Thermal diffusivity (m²/s)
Inhibitor content (%)
Inhibited by N2
Inhibited by CO2
φ = 0 %
φ = 20 %
φ = 50 %
φ = 80 %

Fig. 8

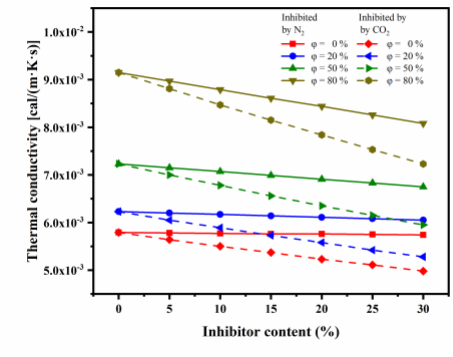
Thermal conductivity [cal/(m·K·s)]
Inhibitor content (%)
Inhibited by N2
Inhibited by CO2
φ = 0 %
φ = 20 %
φ = 50 %
φ = 80 %

Fig. 9

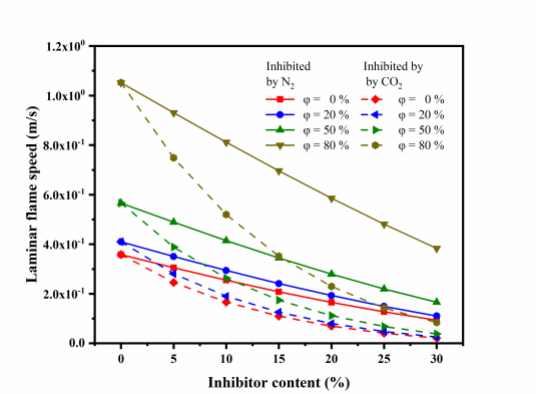

Fig. 10

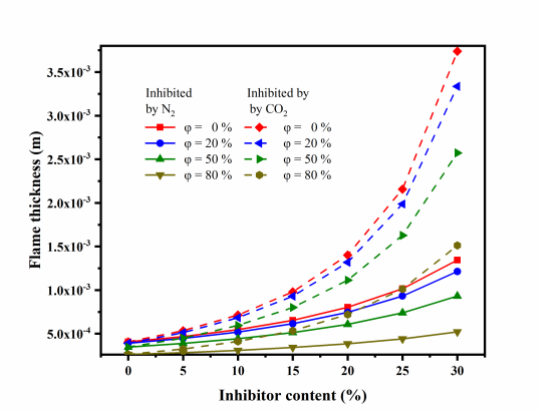

Fig. 11